JACS Au
AN OPEN ACCESS JOURNAL OF THE AMERICAN CHEMICAL SOCIETY

pubs.acs.org/jacsau
Article

Diversity in Atomic Structures of Zeolite-Templated Carbons and the Consequences for Macroscopic Properties

Seunghyuck Chi, Chaehoon Kim, Yongjin Lee,* and Minkee Choi*

Cite This: JACS Au 2024, 4, 1489−1499
Read Online

ACCESS | Metrics & More | Article Recommendations | Supporting Information

ABSTRACT: Zeolite-templated carbons (ZTCs) are a family of ordered microporous carbons with extralarge surface areas and micropore volumes, which are synthesized by carbon deposition within the confined spaces of zeolite micropores. There has been great controversy regarding the atomic structures of ZTCs, which encompass two extremes: (1) three-dimensionally connected curved open-blade-type carbon moieties and (2) ideal tubular structures (commonly referred to as "Schwarzites"). In this study, through a combination of experimental analyses and theoretical calculations, we demonstrate that the atomic structure of ZTCs is difficult to define as a single entity, and it widely varies depending on their synthesis conditions. Carbon deposition using a large organic precursor and low-temperature framework densification generates ZTCs predominantly composed of open-blade-type moieties, characterized by low surface curvature and abundant H-terminated edge sites. Meanwhile, synthesis using a small precursor with high-temperature densification produces ZTCs with an increased portion of closed-strut carbon moieties (or closed-fullerene-like nodes), exhibiting large surface curvature and diminished edge sites. The variations in the atomic structure of ZTCs result in significant differences in their macroscopic properties, such as N_2/CO_2 adsorption, oxidative stability, work function, and electrocatalytic properties, despite the presence of comparable pore structures. Therefore, ZTCs demonstrate the potential to synthesize ordered nanoporous carbons with tunable physicochemical properties.

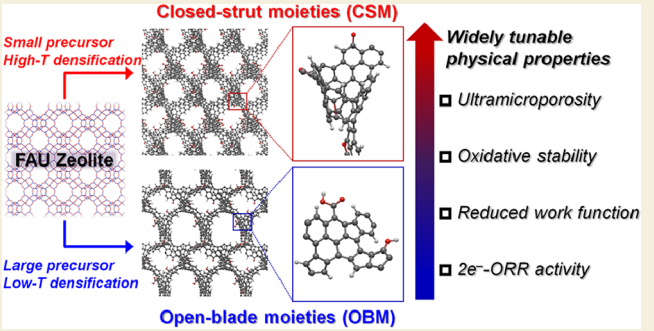

KEYWORDS: *zeolite-templated carbon, atomic structure, surface curvature, work function, oxygen reduction reaction*

INTRODUCTION

Zeolite-templated carbons (ZTCs) refer to a family of ordered microporous carbons synthesized through the replication of zeolites with carbon.[1,2] These materials are created by carbonizing various organic precursors within the confined space of zeolite micropores.[3−5] Large-pore zeolites with ≥12-membered ring pore apertures (diameter ≥0.7 nm) are typically used as templates, as they produce robust, interconnected carbon networks after zeolite dissolution.[6] In principle, the framework and pore connectivity of ZTCs can be tailored based on the structures of the initial zeolite templates. Three-dimensional (3D) carbon structures have been synthesized using FAU,[1−5] *BEA,[6,7] and EMT zeolites as templates,[8] while a two-dimensional (2D) carbon structure has also recently been produced using an IWV zeolite.[9] Due to their uniform micropore diameter, huge specific surface area (up to 3900 $m^2\ g^{-1}$), large micropore volume (up to 1.8 $cm^3\ g^{-1}$), and good electronic conductivity, ZTCs have garnered extensive attention for a wide range of applications, including hydrogen[7,10,11] and methane storage,[12−14] catalysts,[15,16] catalyst supports,[17−19] supercapacitors,[20,21] and membrane fabrication.[9]

Significant efforts have been made to understand the atomic structures of ZTCs.[22−28] Because of carbon deposition within the highly confined zeolite micropores, ZTC frameworks are expected to exhibit high surface curvature and lack conventional graphite-like layer stacking. Nevertheless, due to their amorphous framework nature, unambiguous structural characterization is extremely challenging, resulting in significant controversy regarding the atomic structures of ZTCs. At one extreme, ZTC frameworks are hypothesized as a 3D tubular carbon networks, commonly known as Schwarzites (Scheme 1a).[23−25] Schwarzites are theoretical structures characterized by a triply periodic minimal surface with negative Gaussian curvature, and they are anticipated to exhibit extraordinary physical properties.[29,30] However, experimentally characterized ZTC structures have shown significant disparities in properties compared with the ideal structures of Schwarzites. For

Received: January 8, 2024
Revised: March 6, 2024
Accepted: March 6, 2024
Published: March 29, 2024

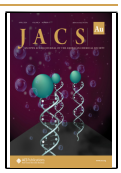

Scheme 1. Schematic Illustration of the Possible Atomic Structure of ZTCs; (a) 3D Closed-Strut-Type Carbon Networks (Schwarzites); (b) 3D Open-Blade-Type Carbon Networks; (c) 3D Open-Blade-Type Carbon Networks with Partially Formed Closed-Strut Moieties

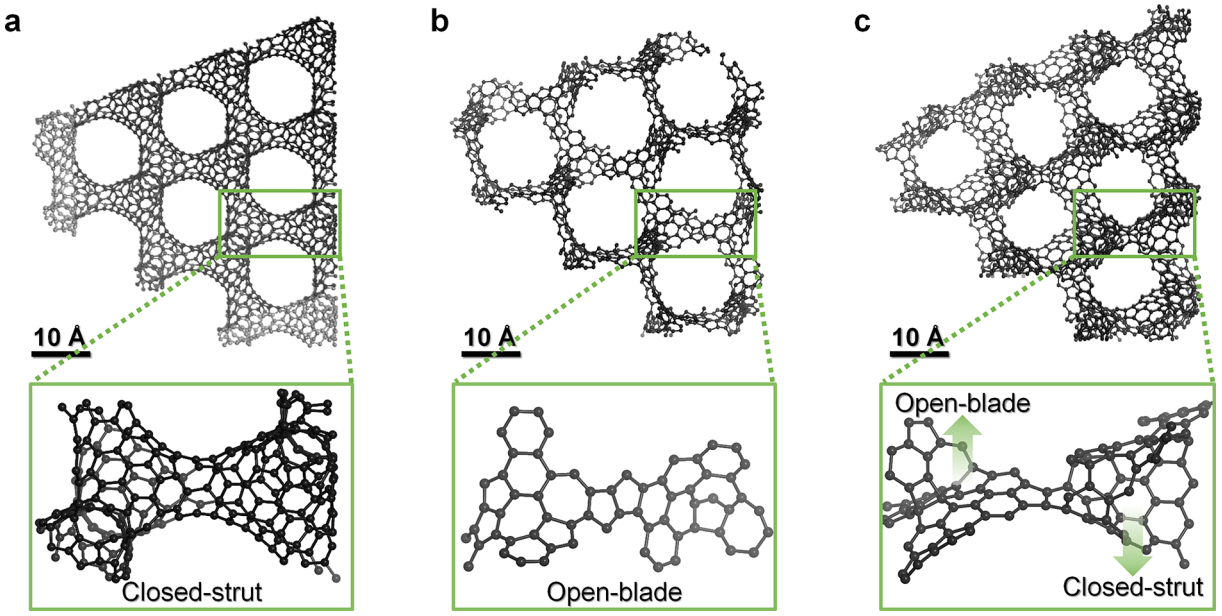

instance, to create a tubule-like carbon framework within FAU zeolite, a high carbon packing density of 0.62−0.68 g_{carbon} $g_{zeolite}^{-1}$ is required,[23,25] which is more than twice the typical experimental values (~0.3 g_{carbon} $g_{zeolite}^{-1}$).[26] In addition, similar to carbon nanotubes, ideal Schwarzites should not have hydrogen (H)- or oxygen (O)-terminated carbon edge sites, and their H and O contents should be negligible. However, ZTCs generally contain substantial amounts of H and O.

On the other extreme, Nishihara and coworkers proposed that ZTCs are better described as 3D interconnected curved open-blade-type carbon moieties (Scheme 1b).[26] This model provides a better explanation for the experimental carbon packing densities and the presence of a large number of carbon edge sites terminated with H and O atoms. Later, the same group proposed more realistic models by introducing increased structural heterogeneity.[27,28] These models can be described as a 3D interconnected carbon framework consisting of diverse open-blade-type carbon moieties with partially formed closed-strut moieties (or closed-fullerene-like nodes; Scheme 1c). This model can be considered an intermediate between the aforementioned two distinct models.

Earlier studies have generally attempted to model the structure of ZTC based on the most commonly reported physical properties in the literature.[26−28] However, careful analysis of previous synthesis results indicates that the structural properties of ZTCs, such as carbon packing density, porous structures (micropore volume and surface area), and the amount of carbon edge sites (or H and O contents), can significantly vary depending on their synthesis conditions.[3,20,31,32] This implies that the atomic structure of ZTCs cannot be described by a single structural model. Instead, within the highly heterogeneous structures of ZTCs, the proportions of open-blade moieties (OBM) and closed-strut moieties (CSM) are likely to change depending on their synthesis conditions.

In the present study, we synthesized a series of ZTCs with a wide range of carbon packing densities (0.26−0.36 g_{carbon} $g_{zeolite}^{-1}$) and carbon edge amounts (H/C atomic ratio = 0.18−0.27) using different organic precursors and thermal densification temperatures. Rigorous material characterization was conducted by combining X-ray diffraction, N_2 and CO_2 adsorption, electron microscopy, Raman spectroscopy, computational modeling, derivative thermogravimetric analysis, ultraviolet photoelectron spectroscopy, and electrocatalytic oxygen reduction reaction. The results demonstrate that the atomic structure of ZTCs significantly varies depending on the synthesis conditions, leading to remarkable differences in their macroscopic properties, such as oxidative stability, work function, and electrocatalytic properties. A comprehensive understanding of the correlation between the atomic structures and macroscopic physicochemical properties of ZTCs would empower us to design novel nanoporous carbons with desired characteristics.

RESULTS AND DISCUSSION

ZTCs were synthesized through the chemical vapor deposition (CVD) of three different organic precursors with varying molecular sizes: acetylene (kinetic diameter: 0.33 nm), ethylene (0.42 nm), and propylene (0.45 nm). Given that the reactivity of the organic precursors decreases in the order of acetylene > propylene > ethylene, we increased the precursor concentration in the following order: acetylene (2%) < propylene (10%) < ethylene (20%) to ensure a reasonable CVD time for ZTC synthesis at 873 K. The carbon deposition was carried out on Ca^{2+}-exchanged Y zeolite (Si/Al = 2.55) because the Ca^{2+} exchange increases the zeolite acidity. This facilitates the polymerization/carbonization of the precursors and enhances the affinity between zeolite micropore surfaces and carbon deposits.[4,8]

In Figure 1a, the residual micropore volume of the zeolite is plotted as a function of the CVD time and carbon packing density (w_c). The results indicate that carbon packing density at full filling of the zeolite micropores decreases in the order of CVD using acetylene (0.36 g_{carbon} $g_{zeolite}^{-1}$) > ethylene (0.30 g_{carbon} $g_{zeolite}^{-1}$) > propylene (0.26 g_{carbon} $g_{zeolite}^{-1}$). This can be

https://doi.org/10.1021/jacsau.4c00028
JACS Au 2024, 4, 1489−1499

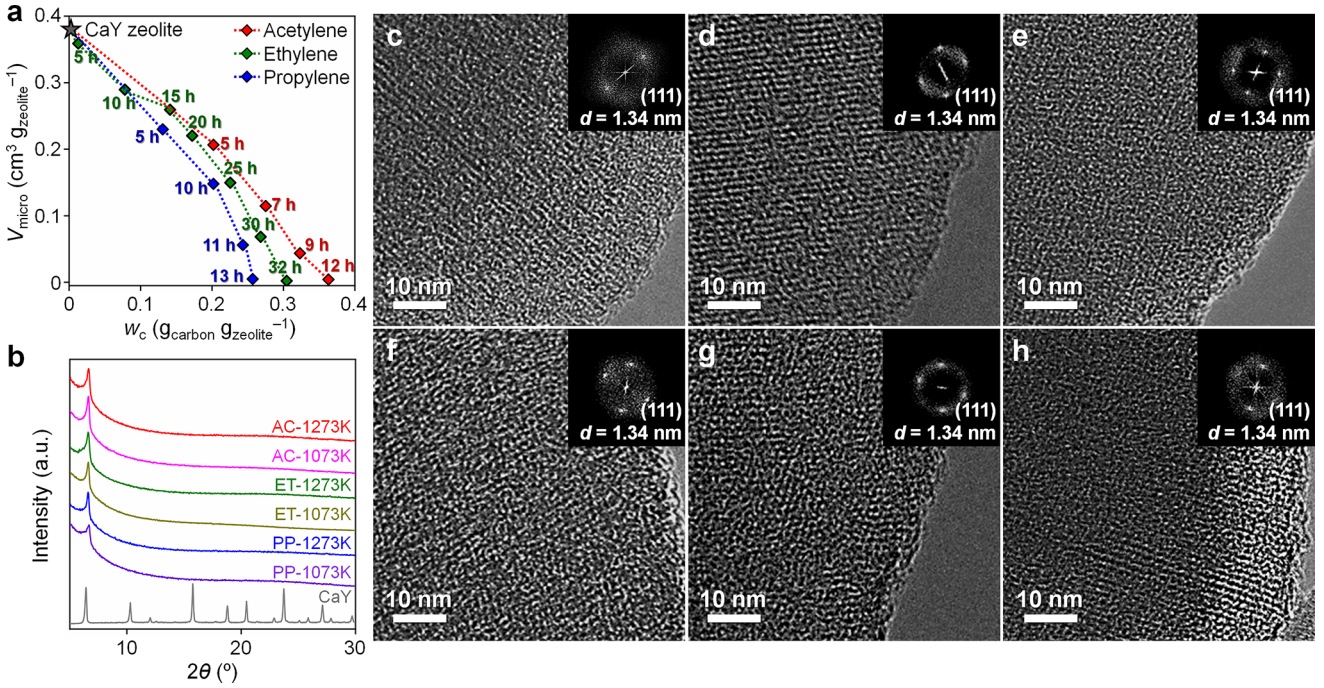

Figure 1. (a) Residual micropore volume of CaY zeolite plotted as a function of CVD time and the carbon packing densities (w_c) during CVD at 873 K using 2% acetylene/Ar (red), 20% ethylene/Ar (green), and 10% propylene/Ar (blue). (b) XRD patterns of ZTCs and CaY. TEM images and Fourier diffractograms (insets) of (c) PP-1073K, (d) ET-1073K, (e) AC-1073K, (f) PP-1273K, (g) ET-1273K, and (h) AC-1273K.

interpreted as utilizing a smaller organic precursor in CVD being advantageous for a continuous supply of a carbon source into zeolite micropores during ZTC synthesis, resulting in a higher carbon packing density. The carbon/zeolite composites with complete micropore filling (CVD times for acetylene, ethylene, and propylene were 12, 32, and 13 h, respectively) were subsequently subjected to thermal framework densification at two different temperatures, 1073 and 1273 K, in an Ar atmosphere. The densification process is essential to obtain ordered microporous carbon structures after zeolite dissolution. We confirmed that the carbon packing density did not change appreciably after thermal densification (Figure S1) because hydrogen atoms were primarily removed during this process. The resulting composites were treated with an HF/HCl aqueous solution to obtain freestanding ZTCs. The ZTC samples were denoted as "*x*–*y*K," where *x* represents the organic precursors (AC: acetylene, ET: ethylene, and PP: propylene), and *y* represents the thermal densification temperature.

In X-ray diffraction (XRD) (Figure 1b), all ZTC samples exhibited a sharp peak at 2θ = 6.6° (corresponding to a *d*-spacing of 1.34 nm), which originates from the (111) structural regularity of the CaY zeolite with a FAU topology. The peak indicates the highly ordered microporous structures of the ZTCs. All ZTCs showed no detectable diffraction peak at 2θ = 24–26°, indicating the negligible formation of dense carbon with graphite-like layer stacking on the zeolite external surface.[12,21] The absence of dense external carbon was further confirmed by a unitary temperature distribution for carbon oxidation at 700–800 K in derivative thermogravimetry (DTG) analyses (Figure S2). In contrast, ZTC deliberately synthesized via carbon overdeposition to additionally contain dense external carbon (denoted as "AC-1073K-ext") exhibited an additional oxidation peak at 820 K (Figure S2). This high-temperature peak can be attributed to the oxidation of dense external carbon.[21] Transmission electron microscopy (TEM) images showed clear lattice fringes for all synthesized ZTCs, confirming their highly ordered microporous structures (Figure 1c–h). In the TEM images, dense carbon layers were not observed at the outer rim of all ZTC particles, which is consistent with the DTG results. These results support that all of the used CVD conditions have produced highly ordered microporous carbons without the formation of dense external carbon.

It is noteworthy that insufficient carbon filling within zeolite micropores results in poor interconnection of the carbon framework and thus the formation of disordered (or collapsed) ZTC structures.[33] Conversely, excessive carbon deposition leads to the development of dense external carbon on the surfaces of ZTCs. The copresence of these nonideal carbon structures hinders the accurate characterization of true ZTC structures. Therefore, the present highly ordered ZTCs without dense external carbon can serve as ideal model systems for understanding the effects of different synthesis conditions on the ZTC pore and framework structures.

All ZTC samples exhibited type I N_2 adsorption–desorption isotherms (Figure 2a), indicating the predominant presence of micropores. According to the nonlocal density functional theory (NLDFT) calculations, the samples exhibited uniform micropore size distributions centered around ~1.2 nm (Figure S3). The ZTC samples showed Brunauer–Emmett–Teller (BET) surface areas ranging from 2562 to 3676 m^2 g^{-1} and micropore volumes ranging from 1.00 to 1.54 cm^3 g^{-1} (Table 1). This wide variation is significant, considering that all ZTC samples show good structural order and the absence of dense external carbon. Both the BET surface area and micropore volume decreased when using a smaller organic precursor and a higher densification temperature (PP-1073K > PP-1273K > ET-1073K > ET-1273K > AC-1073K > AC-1273K). Notably, when the surface areas and micropore volumes were

https://doi.org/10.1021/jacsau.4c00028
JACS Au 2024, 4, 1489–1499

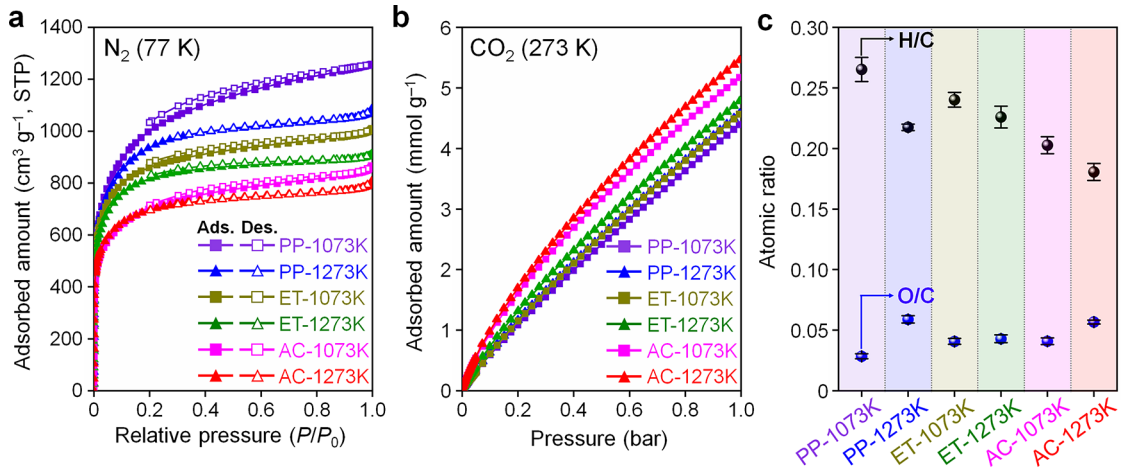

Figure 2. (a) N_2 adsorption−desorption isotherms of ZTCs at 77 K. (b) CO_2 adsorption isotherms of ZTCs at 273 K. (c) H/C (black circle) and O/C (blue circle) atomic ratios of ZTCs.

Table 1. Textural Properties of the ZTC Samples

sample	S_{BET}[a] (m^2 g^{-1})	V_{micro,N_2}[b] (cm^3 g^{-1})	V_{micro,CO_2}[c] (cm^3 g^{-1})	V_{total}[d] (cm^3 g^{-1})	pore size[e] (nm)	H/C atomic ratio	O/C atomic ratio
PP-1073K	3676	1.54	0.21	1.92	1.16	0.27	0.03
PP-1273K	3452	1.34	0.23	1.63	1.16	0.22	0.06
ET-1073K	3121	1.32	0.24	1.53	1.16	0.24	0.04
ET-1273K	2988	1.22	0.25	1.38	1.16	0.23	0.04
AC-1073K	2569	1.02	0.29	1.30	1.24	0.20	0.04
AC-1273K	2562	1.00	0.31	1.20	1.24	0.18	0.06

[a]BET surface areas calculated from N_2 adsorption isotherms determined in the P/P_0 range of 0.05−0.15. [b]Micropore volumes calculated from N_2 adsorption isotherms using the Dubinin−Radushkevich (DR) equation. [c]Ultramicropore volumes calculated from CO_2 adsorption isotherms using DR equation. [d]Total pore volumes determined from N_2 adsorption isotherms at the P/P_0 of 0.96. [e]Pore sizes calculated from N_2 adsorption isotherms using the NLDFT analysis.

normalized by the mass of the initial zeolite template used for CVD (rather than the mass of the resulting carbon), all ZTC samples exhibited remarkably similar values (Figure S4). This suggests that the zeolite micropore surface and framework were faithfully transcribed into the carbon surface and micropore, respectively. Thus, substantial variation in the surface areas and micropore volumes of ZTCs likely originates from the different densities of a carbon framework that is inaccessible to N_2 at 77 K.

In this context, the micropore structures of the ZTC samples were further analyzed using CO_2 adsorption at 273 K (Figure 2b). In the case of very narrow carbon micropores (ultramicropores; diameter <1 nm), N_2 adsorption at 77 K is hardly measurable due to diffusion limitations of N_2 (kinetic diameter: 0.36 nm) molecules at the cryogenic temperature. In contrast, the adsorption of smaller CO_2 molecules (kinetic diameter: 0.33 nm) at an elevated temperature (273 K) can circumvent such diffusion problems.[34] Notably, the CO_2 uptakes corresponding ultramicropore volumes increased in the order of PP-1073K < PP-1273K < ET-1073K < ET-1273K < AC-1073K < AC-1273K (Figure 2b and Table 1), which is completely opposite to the trend of micropore volumes determined by N_2 adsorption at 77 K. These results confirm that the ZTC samples synthesized using a smaller organic precursor and a higher densification temperature contain more ultramicropores that are inaccessible to N_2. Such ultramicropores likely originate from the presence of a less accessible CSM rather than a highly accessible two-sided OBM in the ZTC framework. NLDFT analysis of the CO_2 adsorption isotherms indicated that the size of ultramicropores is centered at approximately 0.6 nm for all ZTC samples (Figure S5).

Elemental analysis of ZTCs (Figure 2c and Table 1) revealed a decrease in the H/C atomic ratios from 0.27 to 0.18 when a smaller organic precursor and a higher densification temperature were employed in their synthesis. This indicates a decrease in the amount of H-terminated carbon edge sites. Conversely, the O/C ratio (or the amount of O-terminated edge sites) was always kept low (O/C = 0.03−0.06), and the proportions of various oxygen functional groups determined by temperature programmed decomposition-mass spectroscopy (TPD-MS) were similar for all samples (Figures S6 and S7 and Table S1). The present results demonstrate that when a smaller organic precursor and a higher densification temperature are employed for ZTC synthesis, the resulting ZTC exhibits a higher carbon packing density, larger ultramicroporosity, and lower amount of H-terminated carbon edge sites. All of these results coherently support the idea that ZTCs synthesized under these conditions comprise more CSM.

To gain additional insights into the carbon building units, we treated AC-1273K, the sample expected to have the largest portion of CSM, with H_2 at 873 K. After the treatment, the H/C atomic ratio slightly increased from 0.18 to 0.19. Meanwhile, the ultramicropore volume determined from CO_2 adsorption decreased from 0.31 to 0.25 cm^3 g^{-1} (Figure S8a), whereas the micropore volume determined from N_2 adsorption increased from 1.00 to 1.03 cm^3 g^{-1} (Figure S8b). These results imply

https://doi.org/10.1021/jacsau.4c00028
JACS Au 2024, 4, 1489−1499

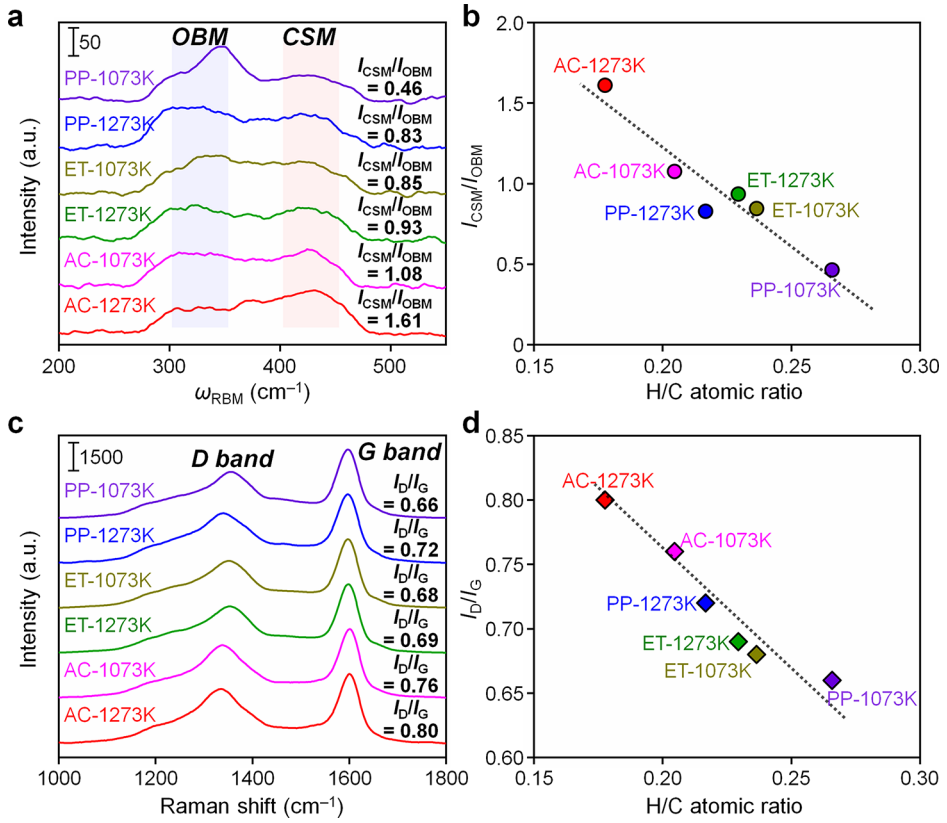

Figure 3. (a) Low-frequency Raman spectra of ZTCs. (b) I_{CSM}/I_{OBM} ratios of RBM bands plotted as a function of the H/C atomic ratios of ZTCs. (c) High-frequency Raman spectra of ZTCs. (d) I_D/I_G ratios plotted as a function of the H/C atomic ratios of ZTCs.

that some of the initially N_2-inaccessible ultramicropores became accessible, likely due to the opening or unzipping of the CSM through H-termination. It is not surprising that certain CSM in ZTCs have very high surface curvature and stress, making them prone to unzipping upon H_2 treatment at 873 K.

To investigate the local structures of ZTCs in greater detail, Raman spectra were analyzed. In the low-frequency Raman spectra (Figure 3a), ZTCs exhibited bands at 270−480 cm^{-1}, which can be attributed to radial breathing mode (RBM) vibrations. These bands are observed in carbon materials with high surface curvatures, such as carbon nanotubes (CNTs),[35,36] nanostructured graphitic materials,[37−39] and ZTCs.[26,40] Two major bands could be distinguished for the ZTC samples: one at 400−450 cm^{-1} and the other at 300−350 cm^{-1}. Since the frequencies of RBM bands (ω_{RBM}) are proportional to the surface curvature of carbon,[39,41] these bands were assigned to CSM with extremely high surface curvature and OBM with relatively low surface curvature, respectively. With the use of a smaller organic precursor and a higher densification temperature, the intensity ratio of the two peaks (I_{CSM}/I_{OBM}) progressively increased: PP-1073K (I_{CSM}/I_{OBM} = 0.46) < PP-1273K (I_{CSM}/I_{OBM} = 0.83) < ET-1073K (I_{CSM}/I_{OBM} = 0.85) < ET-1273K (I_{CSM}/I_{OBM} = 0.93) < AC-1073K (I_{CSM}/I_{OBM} = 1.08) < AC-1273K (I_{CSM}/I_{OBM} = 1.61). These results confirm that using a smaller organic precursor and a higher densification temperature forms ZTCs composed of a larger fraction of CSM. In addition, the intensity ratio of RBM bands (I_{CSM}/I_{OBM}) exhibited an inverse relationship with the H/C ratio of ZTCs (Figure 3b), consistent with the idea that OBM should contain more H-terminated carbon edge sites than CSM.[22]

The high-frequency Raman spectra of ZTCs in the range of 1000−1800 cm^{-1} are shown in Figure 3c. The G band at 1600 cm^{-1} arises from the in-plane stretching vibrations of sp^2-hybridized carbons in a hexagonal lattice structure. The G bands of ZTCs are blue-shifted compared to that of graphite (1580 cm^{-1}), which indicates that the ZTC frameworks are composed of nanosized carbon domains[42,43] without graphite-like layer stacking.[44] The D band at 1350 cm^{-1} originates from the vibrational modes associated with disordered carbon structures, such as lattice defects, carbon edges, and other forms of structural imperfections.[45−48] The intensity ratio of the D and G bands (I_D/I_G) increased with a decreasing H/C ratio of the ZTCs (Figure 3d). It appears that the increased presence of CSM with higher surface curvature results in increased structural disorder. Except for perfectly cylindrical surfaces, the generation of high surface curvature requires carbon polygons other than hexagons, such as pentagons (for positive curvature) and heptagons (for negative curvature). Consequently, the pronounced presence of CSM is likely to generate more structural disorders due to the increased presence of diverse polygons, thus strengthening the D band.

We theoretically constructed structural models for all the synthesized ZTCs (Figures 4 and S9) to reflect their carbon packing densities, H/C and O/C atomic ratios, and oxygen functional group distributions (Tables S2 and S3). The resulting carbon structures are composed predominantly of sp^2-hybridized carbons, and as grown within the confined micropores, they lack conventional graphite-like layer stacking. ZTCs synthesized using a smaller organic precursor and a

https://doi.org/10.1021/jacsau.4c00028
JACS Au 2024, 4, 1489−1499

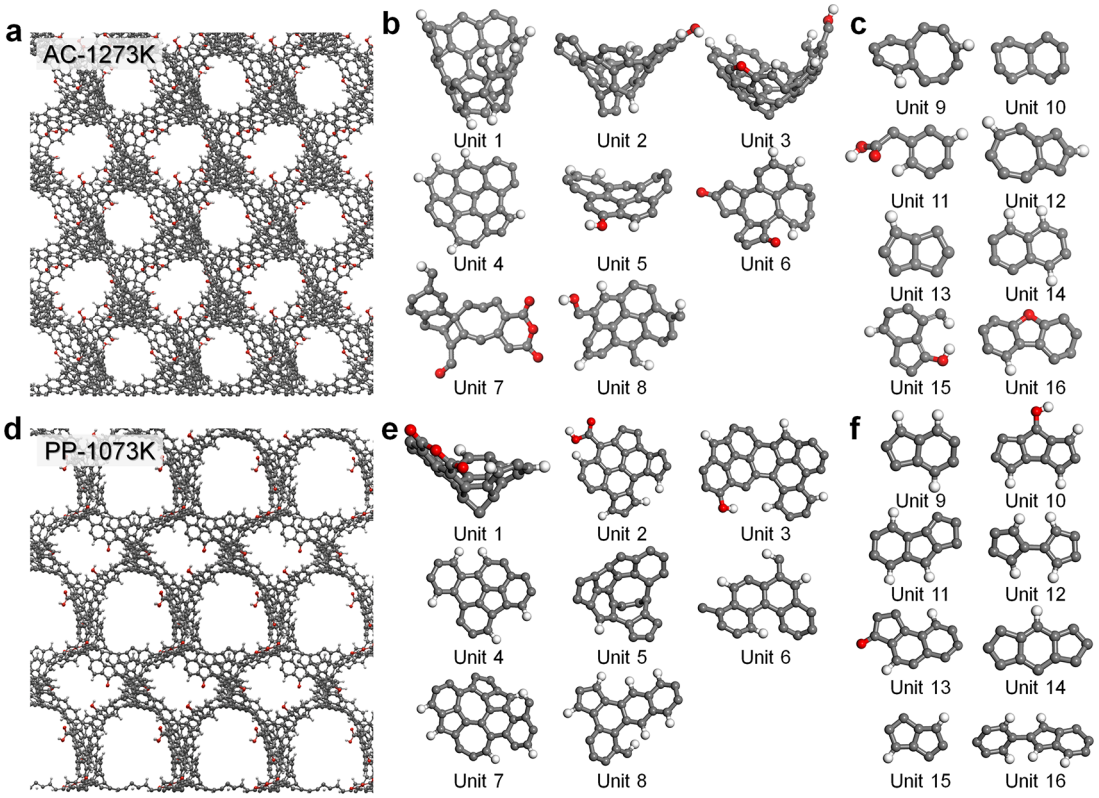

Figure 4. Theoretical ZTC models of (a−c) AC-1273K and (d−f) PP-1073K. Multiunit structures (a,d) and their representative framework units formed within supercages (b,e) and pore necks (c,f) of FAU zeolite.

higher densification temperature are predicted to contain a greater number of CSM. Consequently, AC-1273K possesses the largest number of CSM (units 1−3, Figure 4b), whereas PP-1073K contains the smallest number (only unit 1, Figure 4e). It is noteworthy that even in the case of AC-1273K, CSM appears to form only within the large supercage (internal diameter: 1.3 nm) of the FAU zeolite template (refer to Figure S10 for the zeolite structure). At the narrower pore neck connecting the adjacent supercages (diameter: 0.73 nm), only small naphthalene- or anthracene-like moieties could form as a connecting carbon unit (Figure 4c,f). This result implies that Schwarzites (an ideal 3D carbon tubular structure) are unlikely to form within the FAU zeolite structure. The ZTC models exhibited Gaussian curvature distributions centered around a slightly negative curvature close to zero (Figure S11). The distributions became broader in the models with increased proportions of the CSM, indicating higher local surface curvatures. The simulated adsorption isotherms of the theoretical models were generated using grand canonical Monte Carlo (GCMC) simulations for N_2 at 77 K and CO_2 at 273 K (Figure S12). The N_2 adsorption amounts decreased when using a smaller organic precursor and a higher densification temperature for ZTC synthesis, whereas the CO_2 adsorption amounts increased. These results are consistent with the experimental observations (Figure 2a,b). The GCMC simulations also confirmed that the narrow spaces within the CSM with high surface curvatures offer the strongest adsorption sites for CO_2.

We additionally conducted a comparison of the H/C atomic ratios and carbon packing densities of the synthesized ZTC samples with the anticipated values derived from various theoretical models previously proposed (Figure S13). The results support that all ZTCs synthesized in the present study are still primarily composed of the OBM rather than CSM, and thus, their overall properties are significantly distant from the ideal tubular structures of Schwarzites.

The variations in the atomic structures of ZTCs may give rise to substantial differences in their macroscopic properties. We assessed the oxidative stability and work function of ZTCs through DTG analyses (Figure 5a) and ultraviolet photoelectron spectroscopy (UPS) (Figure 5c), respectively. In the DTG analyses, the temperature for carbon oxidation (T_{ox}) gradually increased with the use of a smaller organic precursor and a higher densification temperature or with decreasing H/C atomic ratios (Figure 5b). These results indicate that ZTC frameworks with a higher proportion of CSM exhibit enhanced stability against oxidation. This can be explained by the fact that OBM contains a significant amount of H-terminated carbon edge sites, which are more susceptible to oxidation compared to in-plane carbon atoms.[49] From the UPS spectra (Figure 5c), the work functions of ZTCs were determined by analyzing the secondary electron cutoff energies (E_{cutoff}). The ZTCs exhibited a wide range of work functions (4.56−5.19 eV), which gradually decreased with the use of a smaller organic precursor and higher densification temperature or decreasing H/C atomic ratios (Figure 5d). These results show that a higher proportion of the CSM results in a reduction in the work function.

Finally, the electrocatalytic oxygen reduction reaction (ORR) properties of ZTCs were evaluated using a rotating ring disk electrode (RRDE) in an O_2-saturated 0.1 M KOH electrolyte. The ORR polarization curves indicated significant variation in catalytic activity across the ZTC samples (Figure 6a). The onset potentials determined at a current (i) of −0.01

https://doi.org/10.1021/jacsau.4c00028
JACS Au 2024, 4, 1489−1499

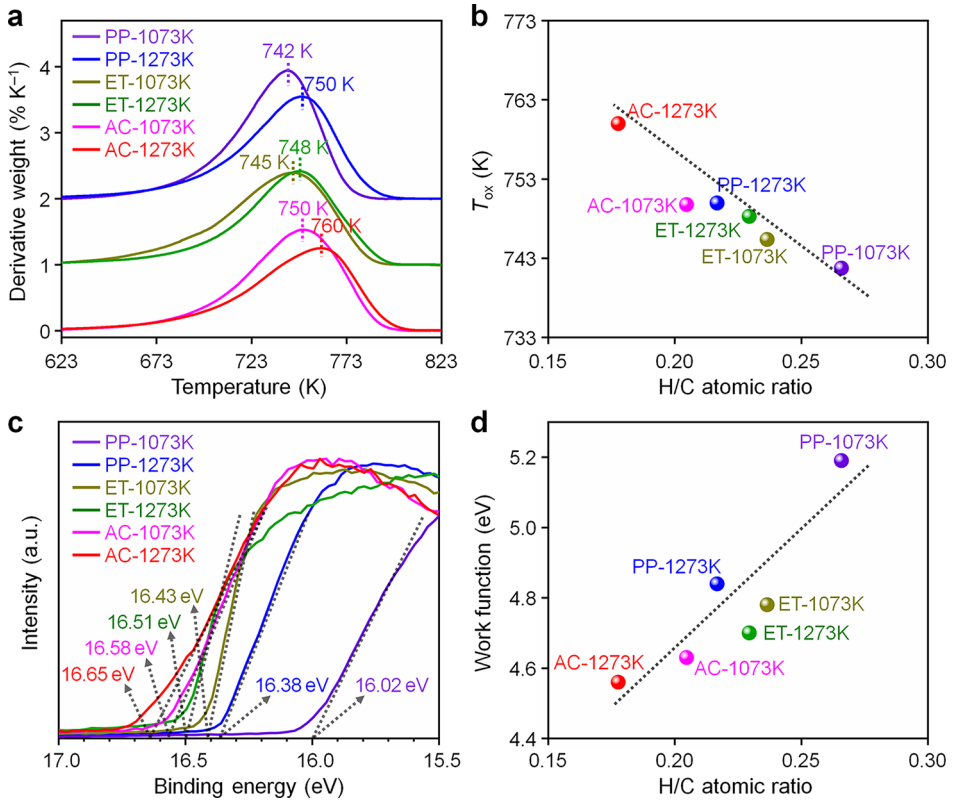

Figure 5. (a) DTG curves of ZTCs measured at a ramping rate of 0.5 K min^{-1} in air. (b) Oxidation temperature (T_{ox}) plotted as a function of the H/C atomic ratios of ZTCs. (c) UPS spectra of ZTCs (secondary electron cutoff energies are indicated). (d) Work functions plotted as a function of the H/C atomic ratios of the ZTCs.

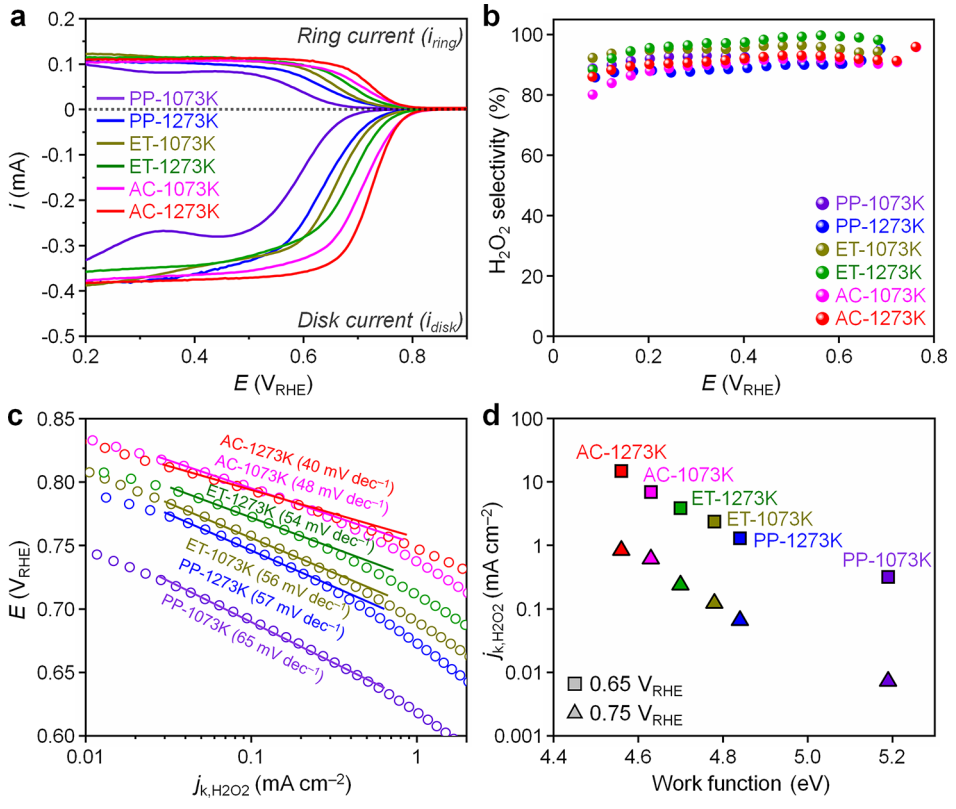

Figure 6. (a) ORR polarization curves and (b) H_2O_2 selectivity of ZTCs measured in O_2-saturated 0.1 M KOH electrolyte. (c) Tafel plots of ZTCs for ORR (Tafel slopes are indicated). (d) Kinetic current densities (j_{k,H_2O_2}) at 0.65 and 0.75 V_{RHE} plotted as a function of the work functions of the ZTCs.

https://doi.org/10.1021/jacsau.4c00028
JACS Au 2024, 4, 1489−1499

mA exhibited a gradual increase from 0.69 to 0.79 V_{RHE} with the use of a smaller organic precursor and higher densification temperature or with decreasing H/C ratios. Meanwhile, the half-wave potentials increased from 0.57 V_{RHE} to 0.72 V_{RHE}. These results indicate that ZTCs with a larger proportion of CSM exhibit higher ORR activities. All ZTCs exhibited a predominant production of hydrogen peroxide (H_2O_2) with a selectivity exceeding 85%, indicative of a two-electron ORR pathway (Figure 6b).

In the Tafel plots (Figure 6c), ZTCs with a larger proportion of CSM exhibited smaller Tafel slopes, indicating a lower activation energy for the rate-determining step. It has been reported that the first electron transfer from the carbon surface to O_2, resulting in the formation of hydroperoxo (OOH) species, is the rate-determining step in the two-electron ORR over metal-free carbon catalysts.[50] Notably, both of the kinetic current densities (j_{k,H_2O_2}) measured at 0.65 and 0.75 V_{RHE} exhibited an inverse relationship with the work functions of ZTCs (Figure 6d). This can be attributed to the fact that the low work functions of carbon catalysts are beneficial in facilitating the first electron transfer to O_2, thereby increasing ORR activity.[51,52] As a result, AC-1273K exhibited a 116-fold higher j_{k,H_2O_2} value compared to PP-1073K at 0.75 V_{RHE} (46-fold higher at 0.65 V_{RHE}). The observed H_2O_2 electrosynthesis activity is comparable to that of the state-of-the-art carbon catalysts reported in the literature (Figure S14).

CONCLUSIONS

We synthesized a series of ZTCs with varying carbon packing densities and carbon edge amounts by altering organic precursors and thermal densification temperatures. Rigorous structural characterization, combining experimental and theoretical analyses, demonstrates that the atomic structure of ZTCs significantly varies, depending on their synthesis conditions. The results demonstrate that carbon deposition using a large organic precursor and low-temperature thermal densification generates ZTCs predominantly composed of an OBM, characterized by low surface curvature and abundant H-terminated edge sites. In contrast, synthesis using a small precursor with high-temperature densification produces ZTCs with an increased proportion of CSM, exhibiting a large surface curvature and reduced edge sites. The variation in the atomic structure of ZTCs results in substantial differences in their macroscopic properties, such as oxidative stability, work function, and electrocatalytic properties, despite the similarity of their porous structures. A comprehensive understanding of the correlation between the atomic structures and macroscopic physicochemical properties of ZTCs would enable us to design novel nanoporous carbons with tailored properties.

EXPERIMENTAL SECTION

Synthesis of ZTCs

CaY zeolite was prepared by ion-exchanging NaY (CBV100, Zeolyst International, Si/Al = 2.55) with a 1 M $Ca(NO_3)_2$ (98.5%, Samchun) aqueous solution twice at room temperature. In a typical synthesis of ZTC, 5.0 g of CaY was placed in a quartz plug-flow reactor (inner diameter: 5.5 cm) and heated to 873 K (ramp: 2 K min^{-1}) under Ar flow (200 cm^3 min^{-1}). To synthesize AC-*y*K samples, the gas was switched to 2% acetylene/Ar (400 cm^3 min^{-1}), and CVD was conducted for 12 h. Subsequently, the temperature was increased to 1073 or 1273 K (ramp: 2 K min^{-1}) under Ar flow (200 cm^3 min^{-1}) and held for 3 h to synthesize AC-1073K and AC-1273K, respectively. The resultant carbon/zeolite composites were treated with a 0.3 M HF/0.1 M HCl solution to remove the zeolite template. The resulting ZTCs were collected by filtration, thoroughly washed with deionized water, and dried overnight at 373 K. The acid treatment was repeated twice. Similarly, ET-*y*K and PP-*y*K samples were prepared through CVD under a flow of 20% ethylene/Ar (400 cm^3 min^{-1}) for 32 h and a flow of 10% propylene/Ar (400 cm^3 min^{-1}) for 13 h, respectively. To synthesize ZTC with dense external carbon (AC-1073K-ext), CVD was conducted at 873 K for 12 h under a flow of 2% acetylene/Ar (400 cm^3 min^{-1}), followed by an additional CVD at 1073 K for 4 h.

Material Characterization

The carbon packing densities were determined through thermogravimetric analysis of carbon/zeolite composites using N-1000 (SINCO) with a ramping rate of 10 K min^{-1} under a flow of air (50 cm^3 min^{-1}). DTG curves of ZTCs were collected by using the same equipment with a ramping rate of 0.5 K min^{-1} under a flow of air (50 cm^3 min^{-1}). N_2 adsorption−desorption isotherms were measured using a BELSORP-max (BEL Japan) volumetric analyzer at 77 K. Before measurement, the carbon/zeolite composites were degassed at 673 K for 4 h, and ZTCs were degassed at 523 K for 4 h under vacuum. BET surface areas were calculated in the P/P_0 range of 0.05−0.15. Micropore volumes were calculated using the Dubinin−Radushkevich (DR) equation, and the total pore volumes were determined at a P/P_0 of 0.96. Pore size distributions were calculated by NLDFT analysis, assuming a graphitic carbon with slit-like pore geometry and a single log-normal pore size distribution. CO_2 adsorption isotherms were measured at 273 K using a 3-Flex (Micromeritics) volumetric analyzer. Ultramicropore volumes were calculated using the DR equation, and pore size distributions were calculated by NLDFT analysis, assuming a graphitic carbon with slit-like pore geometry. The H/C and O/C atomic ratios of ZTCs were determined by elemental analysis using a FLASH 2000 (Thermo Scientific). Prior to measurement, ZTCs were thoroughly evacuated at 523 K for 4 h. Each measurement was repeated three times. TPD-MS profiles were collected using a BELMASS II (BEL Japan). Typically, 0.03 g of the sample was heated to 1273 K (ramp: 5 K min^{-1}) under Ar flow (30 cm^3 min^{-1}).

XRD patterns were recorded by using a SmartLab X-ray diffractometer (RIGAKU) equipped with a Cu Kα radiation source (40 kV, 200 mA). TEM investigation was conducted with an FEI Titan Cubed G2 60-300 microscope operating at 200 kV (KAIST Analysis Center for Research Advancement, KARA). Prior to the investigation, the samples were loaded onto a lacey carbon grid (LC300-Cu) by drop-casting an ethanolic dispersion. Raman spectra were recorded using a LabRAM ARAMIS (Horiba Jobin Yvon) with an Ar ion laser (514 nm). UPS analysis was conducted using an Axis-Supra (Kratos) with a He I (21.21 eV) photon source. To minimize the potential influence of adsorbates on the work function,[53] ZTCs were evacuated at 523 K for 4 h before the UPS measurement. Work functions were calculated from the shift in the E_{cutoff}: work function = $h\nu$ (He I photon energy) − E_{cutoff}.

Computational Modeling of ZTC Structures

Fully relaxed ZTC structures were generated through a computational methodology that combines continuous ran-

https://doi.org/10.1021/jacsau.4c00028
JACS Au 2024, 4, 1489−1499

dom network model-based Metropolis Monte Carlo (CRN-MMC) simulations with density functional theory (DFT) calculations. The structure generation began with a seed comprising four carbon atoms (a central atom bonded to three neighbors) positioned within the pore space of the FAU zeolite. With our in-house code, the ZTC structures grew via CRN-MMC simulations utilizing the valence force field specific to sp^2 carbon systems.[54] Carbon-framework interactions reflect Lennard−Jones (LJ) parameters, guided by the Universal force field with the Lorentz−Berthelot mixing rules, and a truncated cutoff of 7.0 Å was applied.

In every simulation cycle, the code executed one of the following moves: inserting a carbon atom into an undercoordinated atom, deleting an existing carbon atom, switching bonds between adjacent atoms, or bond dissociation. Following each move, the new structure underwent a relaxation phase. This structure was accepted if its energy difference, ΔE, with the previous structure was negative or if the Boltzmann factor, $\exp(-\Delta E/kT)$, exceeded a random value between 0 and 1. Structures failing this criterion reverted to their former state. A penalty energy was enforced if the carbon atom count surpassed the experimental carbon density for the samples, and the CRN-MMC simulation ended when the energy reduction became negligible. After the CRN-MMC simulation, the zeolite template was removed, and based on experimentally determined functional group ratios, functional groups were manually introduced to the ZTC edges. Further optimization of the ZTC structures was conducted through DFT calculations, adopting the generalized gradient approximation of Perdew, Burke, and Ernzerhof (PBE).[55] These calculations utilized the Vienna ab initio simulation package (VASP),[56] incorporating a plane-wave basis set and projector-augmented-wave pseudopotentials.[57,58] Wave function energy convergence was set at 10^{-4} eV. Optimization persisted until residual forces reduced below 0.01 eV/Å.

Simulated N_2 and CO_2 adsorption isotherms were obtained using a grand canonical Monte Carlo simulation (GCMC) implemented in RASPA.[59] In all GCMC simulations, the ZTC frameworks were treated as rigid. The ZTC−adsorbate and adsorbate−adsorbate interactions were modeled using the LJ potential with a cutoff distance of 14 Å and tail corrections. For N_2 (or CO_2) adsorption simulation, we adopted the LJ potential parameters for carbon atoms as ε = 28.2 K (or 47.8 K) and σ = 3.4 Å (or 3.47 Å).[60,61] N_2 and CO_2 molecules were described as the TraPPE model.[62] For each GCMC simulation, 2×10^5 MC cycles (the initial 10^5 MC steps for equilibration and the subsequent 10^5 MC cycles for property production steps by running averages) were performed with random translation, rotation, and insertion/deletion moves. Zeo++[63] (with a 1.4 Å probe size) was used to estimate the accessible surface area and void fraction, while SESAMI 2.0[64] was employed to predict the BET surface areas of ZTCs from the GCMC-simulated isotherms.

The local Gaussian curvature of ZTCs was estimated by focusing on all carbon atoms and oxygen atoms connected to two carbon atoms. Using the atomic coordinates, a KDTree was constructed to efficiently determine neighboring atoms within a radius of 3.5 Å. For each atom, a second-order polynomial ($z = a + bx + by + xx^2 + cyy^2 + dxy$) was used to fit the local surface topology using relative coordinates of neighboring atoms. The polynomial coefficients were then used to calculate Gaussian curvature. Atoms with fewer than six neighbors were assigned a Gaussian curvature of zero.

Electrochemical Measurements

Electrochemical experiments were performed by using a VMP3 potentiostat (Bio-Logic). A three-electrode system was equipped with a graphite rod counter electrode and a Hg/HgO (RE-61AP, ALS) reference electrode. As an electrolyte, a 0.1 M KOH aqueous solution was used. All potentials denoted in this study were referenced to the reversible hydrogen electrode (RHE), after calibrating the reference electrode in H_2-saturated electrolyte using a Pt electrode. The catalyst ink was prepared by dispersing 10 mg of the catalyst in a solution containing 7137 μL of ethanol, 27 μL of 5 wt % Nafion solution, and 793 μL of deionized water, followed by sonication for 30 min. The working electrode was prepared by drop-casting 10 μL of the ink onto a glassy carbon disk (0.126 cm^2) of a Pt-ring-disk electrode (A-011162, ALS). The total loading of catalysts was fixed at 100 μg of cm^{-2}. The ORR responses were measured in the potential range of 0.05−1.0 V_{RHE} with a scan rate of 5 mV s^{-1} and a rotation speed of 1600 rpm in the electrolyte saturated with O_2 using the rotator (RRDE-3A, ALS). H_2O_2 selectivity was simultaneously measured with the polarized potential of 1.3 V_{RHE} on the Pt-ring electrode.

■ ASSOCIATED CONTENT

Supporting Information

The Supporting Information is available free of charge at https://pubs.acs.org/doi/10.1021/jacsau.4c00028.

Additional characterization data (DTG curves, N_2 and CO_2 adsorption isotherms, pore size distributions, and TPD-MS results), computational results (theoretical ZTC models and Gaussian curvature distributions), and catalytic performance (PDF)

■ AUTHOR INFORMATION

Corresponding Authors

Yongjin Lee − *Department of Chemistry and Chemical Engineering, Education and Research Center for Smart Energy and Materials, Inha University, Incheon 22212, Republic of Korea;* orcid.org/0000-0001-8166-2935; Email: yongjin.lee@inha.ac.kr

Minkee Choi − *Department of Chemical and Biomolecular Engineering (BK21 Four), Korea Advanced Institute of Science and Technology, Daejeon 34141, Republic of Korea;* orcid.org/0000-0003-0827-2572; Email: mkchoi@kaist.ac.kr

Authors

Seunghyuck Chi − *Department of Chemical and Biomolecular Engineering (BK21 Four), Korea Advanced Institute of Science and Technology, Daejeon 34141, Republic of Korea*

Chaehoon Kim − *Department of Chemical and Biomolecular Engineering (BK21 Four), Korea Advanced Institute of Science and Technology, Daejeon 34141, Republic of Korea*

Complete contact information is available at: https://pubs.acs.org/10.1021/jacsau.4c00028

Author Contributions

M.C. and Y.L. conceived and designed this study. S.C. and C.K. prepared the materials, performed structural and catalytic characterizations, and analyzed the experimental results. Y.L. performed the DFT calculations. All the authors prepared the

https://doi.org/10.1021/jacsau.4c00028
JACS Au 2024, 4, 1489−1499

manuscript together. CRediT: S.C. conceptualization, methodology, formal analysis, investigation, writing − original draft, and writing − review and editing; C.K. formal analysis, investigation, and writing − review and editing; Y.L. methodology, formal analysis, investigation, data curation, and writing − original draft; M.C. conceptualization, methodology, resources, writing − original draft, writing − review and editing, supervision, project administration, and funding acquisition. CRediT: **Seunghyuck Chi** conceptualization, formal analysis, investigation, methodology, writing-original draft, writing-review & editing; **Chaehoon Kim** formal analysis, investigation, writing-review & editing; **Yongjin Lee** data curation, formal analysis, investigation, methodology, writing-original draft; **Minkee Choi** conceptualization, funding acquisition, methodology, project administration, resources, supervision, writing-original draft, writing-review & editing.

Notes

The authors declare no competing financial interest.

■ ACKNOWLEDGMENTS

This work was supported by National Research Foundation of Korea (NRF) grants funded by Korea government (Ministry of Science and ICT; RS-2023-00259416 and 2022M3H4A1A04076372).

■ REFERENCES

(1) Kyotani, T.; Nagai, T.; Inoue, S.; Tomita, A. Formation of New Type of Porous Carbon by Carbonization in Zeolite Nanochannels. *Chem. Mater.* **1997**, *9* (2), 609−615.
(2) Ma, Z.; Kyotani, T.; Tomita, A. Preparation of a High Surface Area Microporous Carbon Having the Structural Regularity of Y Zeolite. *Chem. Commun.* **2000**, *23*, 2365−2366.
(3) Hou, P. X.; Yamazaki, T.; Orikasa, H.; Kyotani, T. An Easy Method for the Synthesis of Ordered Microporous Carbons by the Template Technique. *Carbon* **2005**, *43* (12), 2624−2627.
(4) Kim, K.; Kwon, Y.; Lee, T.; Cho, S. J.; Ryoo, R. Facile Large-Scale Synthesis of Three-Dimensional Graphene-Like Ordered Microporous Carbon via Ethylene Carbonization in CaX Zeolite Template. *Carbon* **2017**, *118*, 517−523.
(5) Park, H.; Bang, J.; Han, S. W.; Bera, R. K.; Kim, K.; Ryoo, R. Synthesis of Zeolite-Templated Carbons Using Oxygen-Containing Organic Solvents. *Microporous Mesoporous Mater.* **2021**, *318*, 111038.
(6) Kyotani, T.; Ma, Z.; Tomita, A. Template Synthesis of Novel Porous Carbons Using Various Types of Zeolites. *Carbon* **2003**, *41* (7), 1451−1459.
(7) Yang, Z.; Xia, Y.; Mokaya, R. Enhanced Hydrogen Storage Capacity of High Surface Area Zeolite-like Carbon Materials. *J. Am. Chem. Soc.* **2007**, *129* (6), 1673−1679.
(8) Kim, K.; Lee, T.; Kwon, Y.; Seo, Y.; Song, J.; Park, J. K.; Lee, H.; Park, J. Y.; Ihee, H.; Cho, S. J.; et al.et al. Lanthanum-Catalysed Synthesis of Microporous 3D Graphene-like Carbons in a Zeolite Template. *Nature* **2016**, *535* (7610), 131−135.
(9) Kim, C.; Koh, D. Y.; Lee, Y.; Choi, J.; Cho, H. S.; Choi, M. Bottom-Up Synthesis of Two-Dimensional Carbon with Vertically Aligned Ordered Micropores for Ultrafast Nanofiltration. *Sci. Adv.* **2023**, *9* (6), No. eade7871.
(10) Stadie, N. P.; Vajo, J. J.; Cumberland, R. W.; Wilson, A. A.; Ahn, C. C.; Fultz, B. Zeolite-Templated Carbon Materials for High-Pressure Hydrogen Storage. *Langmuir* **2012**, *28* (26), 10057−10063.
(11) Nishihara, H.; Hou, P. X.; Li, L. X.; Ito, M.; Uchiyama, M.; Kaburagi, T.; Ikura, A.; Katamura, J.; Kawarada, T.; Mizuuchi, K.; et al.et al. High-Pressure Hydrogen Storage in Zeolite-Templated Carbon. *J. Phys. Chem. C* **2009**, *113* (8), 3189−3196.
(12) Choi, S.; Kim, H.; Lee, S.; Wang, Y.; Ercan, C.; Othman, R.; Choi, M. Large-Scale Synthesis of High-Quality Zeolite-Templated Carbons without Depositing External Carbon Layers. *Chem. Eng. J.* **2015**, *280*, 597−605.
(13) Choi, S.; Alkhabbaz, M. A.; Wang, Y.; Othman, R. M.; Choi, M. Unique Thermal Contraction of Zeolite-Templated Carbons Enabling Micropore Size Tailoring and Its Effects on Methane Storage. *Carbon* **2019**, *141*, 143−153.
(14) Stadie, N. P.; Murialdo, M.; Ahn, C. C.; Fultz, B. Anomalous Isosteric Enthalpy of Adsorption of Methane on Zeolite-Templated Carbon. *J. Am. Chem. Soc.* **2013**, *135* (3), 990−993.
(15) Chung, P. W.; Yabushita, M.; To, A. T.; Bae, Y.; Jankolovits, J.; Kobayashi, H.; Fukuoka, A.; Katz, A. Long-Chain Glucan Adsorption and Depolymerization in Zeolite-Templated Carbon Catalysts. *ACS Catal.* **2015**, *5* (11), 6422−6425.
(16) Han, S. W.; Bang, J.; Ko, S. H.; Ryoo, R. Variation of Nitrogen Species in Zeolite-Templated Carbon by Low-Temperature Carbonization of Pyrrole and the Effect on Oxygen Reduction Activity. *J. Mater. Chem. A* **2019**, *7* (14), 8353−8360.
(17) Choi, C. H.; Kim, M.; Kwon, H. C.; Cho, S. J.; Yun, S.; Kim, H. T.; Mayrhofer, K. J. J.; Kim, H.; Choi, M. Tuning Selectivity of Electrochemical Reactions by Atomically Dispersed Platinum Catalyst. *Nat. Commun.* **2016**, *7* (1), 10922.
(18) Chi, S.; Ji, S. G.; Kim, M.; Kim, H.; Choi, C. H.; Choi, M. Structural Heterogeneity of Single-Atom Catalysts and True Active Site Generation via Ligand Exchange during Electrochemical H_2O_2 Production. *J. Catal.* **2023**, *419*, 49−57.
(19) Ou, Z.; An, Z.; Ma, Z.; Li, N.; Han, Y.; Yang, G.; Jiang, Q.; Chen, Q.; Chu, W.; Wang, S.; et al.et al. 3D Porous Graphene-like Carbons Encaged Single-Atom-Based Pt for Ultralow Loading and High-Performance Fuel Cells. *ACS Catal.* **2023**, *13* (3), 1856−1862.
(20) Itoi, H.; Nishihara, H.; Kogure, T.; Kyotani, T. Three-Dimensionally Arrayed and Mutually Connected 1.2-nm Nanopores for High-Performance Electric Double Layer Capacitor. *J. Am. Chem. Soc.* **2011**, *133* (5), 1165−1167.
(21) Kwon, H. C.; Choi, S.; Wang, Y.; Othman, R.; Choi, M. Scalable Synthesis of Zeolite-Templated Ordered Microporous Carbons without External Carbon Deposition for Capacitive Energy Storage. *Microporous Mesoporous Mater.* **2020**, *307*, 110481.
(22) Taylor, E. E.; Garman, K.; Stadie, N. P. Atomistic Structures of Zeolite-Templated Carbon. *Chem. Mater.* **2020**, *32* (7), 2742−2752.
(23) Roussel, T.; Didion, A.; Pellenq, R. J. M.; Gadiou, R.; Bichara, C.; Vix-Guterl, C. Experimental and Atomistic Simulation Study of the Structural and Adsorption Properties of Faujasite Zeolite−Templated Nanostructured Carbon Materials. *J. Phys. Chem. C* **2007**, *111* (43), 15863−15876.
(24) Roussel, T.; Jagiello, J.; Pellenq, R. J.-M.; Thommes, M.; Bichara, C. Testing the Feasibility of Using the Density Functional Theory Route for Pore size Distribution Calculations of Ordered Microporous Carbons. *Mol. Simul.* **2006**, *32* (7), 551−555.
(25) Braun, E.; Lee, Y.; Moosavi, S. M.; Barthel, S.; Mercado, R.; Baburin, I. A.; Proserpio, D. M.; Smit, B. Generating Carbon Schwarzites via Zeolite-Templating. *Proc. Natl. Acad. Sci. U. S. A.* **2018**, *115* (35), No. E8116−E8124.
(26) Nishihara, H.; Yang, Q. H.; Hou, P. X.; Unno, M.; Yamauchi, S.; Saito, R.; Paredes, J. I.; Martínez-Alonso, A.; Tascón, J. M. D.; Sato, Y.; et al.et al. A Possible Buckybowl-like Structure of Zeolite Templated Carbon. *Carbon* **2009**, *47* (5), 1220−1230.
(27) Nishihara, H.; Fujimoto, H.; Itoi, H.; Nomura, K.; Tanaka, H.; Miyahara, M. T.; Bonnaud, P. A.; Miura, R.; Suzuki, A.; Miyamoto, N.; et al.et al. Graphene-based Ordered Framework with a Diverse Range of Carbon Polygons Formed in Zeolite Nanochannels. *Carbon* **2018**, *129*, 854−862.
(28) Tanaka, H.; Seto, T.; Nishihara, H.; Kyotani, T.; Miyahara, M. T. Synthesis of Zeolite-Templated Carbons for Methane Storage: A Molecular Simulation Study. *Tanso* **2018**, *2018* (285), 197−203.
(29) Lenosky, T.; Gonze, X.; Teter, M.; Elser, V. Energetics of Negatively Curved Graphitic Carbon. *Nature* **1992**, *355* (6358), 333−335.
(30) Mackay, A. L.; Terrones, H. Diamond from Graphite. *Nature* **1991**, *352* (6338), 762.

https://doi.org/10.1021/jacsau.4c00028
JACS Au 2024, 4, 1489−1499

(31) Ma, Z.; Kyotani, T.; Tomita, A. Synthesis Methods for Preparing Microporous Carbons with a Structural Regularity of Zeolite Y. *Carbon* **2002**, *40* (13), 2367−2374.
(32) Aumond, T.; Le Person, A.; Batonneau-Gener, I.; Vezin, H.; Sachse, A.; Moissette, A. Solid-State Synthesis of Zeolite-Templated Carbons. *J. Phys. Chem. C* **2023**, *127* (7), 3486−3496.
(33) Nishihara, H.; Kyotani, T. Zeolite-Templated Carbons − Three-Dimensional Microporous Graphene Frameworks. *Chem. Commun.* **2018**, *54* (45), 5648−5673.
(34) Lozano-Castelló, D.; Cazorla-Amorós, D.; Linares-Solano, A. Usefulness of CO_2 Adsorption at 273 K for the Characterization of Porous Carbons. *Carbon* **2004**, *42* (7), 1233−1242.
(35) Rao, A. M.; Richter, E.; Bandow, S.; Chase, B.; Eklund, P. C.; Williams, K. A.; Fang, S.; Subbaswamy, K. R.; Menon, M.; Thess, A.; et al.et al. Diameter-Selective Raman Scattering from Vibrational Modes in Carbon Nanotubes. *Science* **1997**, *275* (5297), 187−191.
(36) Dresselhaus, M. S.; Eklund, P. C. Phonons in Carbon Nanotubes. *Adv. Phys.* **2000**, *49* (6), 705−814.
(37) Gogotsi, Y.; Libera, J. A.; Kalashnikov, N.; Yoshimura, M. Graphite Polyhedral Crystals. *Science* **2000**, *290* (5490), 317−320.
(38) Wang, J. J.; Zhu, M. Y.; Outlaw, R. A.; Zhao, X.; Manos, D. M.; Holloway, B. C.; Mammana, V. P. Free-Standing Subnanometer Graphite Sheets. *Appl. Phys. Lett.* **2004**, *85* (7), 1265−1267.
(39) Lee, J. K.; Hembram, K. P. S. S.; Park, Y.; Lee, S. G.; Kim, J. G.; Lee, W.; Moon, D. J. Raman Radial Mode Revealed from Curved Graphene. *J. Phys. Chem. Lett.* **2017**, *8* (12), 2597−2601.
(40) Paredes, J. I.; Martinez-Alonso, A.; Yamazaki, T.; Matsuoka, K.; Tascon, J. M. D.; Kyotani, T. Structural Investigation of Zeolite-Templated, Ordered Microporous Carbon by Scanning Tunneling Microscopy and Raman Spectroscopy. *Langmuir* **2005**, *21* (19), 8817−8823.
(41) Jorio, A.; Saito, R.; Hafner, J. H.; Lieber, C. M.; Hunter, D. M.; McClure, T.; Dresselhaus, G.; Dresselhaus, M. S. Structural (n, m) Determination of Isolated Single-Wall Carbon Nanotubes by Resonant Raman Scattering. *Phys. Rev. Lett.* **2001**, *86* (6), 1118.
(42) Ferrari, A. C.; Robertson, J. Interpretation of Raman Spectra of Disordered and Amorphous Carbon. *Phys. Rev. B* **2000**, *61* (20), 14095.
(43) Schüpfer, D. B.; Badaczewski, F.; Peilstöcker, J.; Guerra-Castro, J. M.; Shim, H.; Firoozabadi, S.; Beyer, A.; Volz, K.; Presser, V.; Heiliger, C.; et al.et al. Monitoring the Thermally Induced Transition from sp^3-Hybridized into sp^2-Hybridized Carbons. *Carbon* **2021**, *172*, 214−227.
(44) Das, A.; Chakraborty, B.; Sood, A. K. Raman Spectroscopy of Graphene on Different Substrates and Influence of Defects. *Bull. Mater. Sci.* **2008**, *31*, 579−584.
(45) Katagiri, G.; Ishida, H.; Ishitani, A. Raman Spectra of Graphite Edge Planes. *Carbon* **1988**, *26* (4), 565−571.
(46) Dresselhaus, M. S.; Jorio, A.; Souza Filho, A. G.; Saito, R. Defect Characterization in Graphene and Carbon Nanotubes Using Raman Spectroscopy. *Philos. Trans. R. Soc., A* **2010**, *368* (1932), 5355−5377.
(47) Jia, Y.; Zhang, L.; Du, A.; Gao, G.; Chen, J.; Yan, X.; Brown, C. L.; Yao, X. Defect Graphene as a Trifunctional Catalyst for Electrochemical Reactions. *Adv. Mater.* **2016**, *28* (43), 9532−9538.
(48) Wu, Q.; Jia, Y.; Liu, Q.; Mao, X.; Guo, Q.; Yan, X.; Zhao, J.; Liu, F.; Du, A.; Yao, X. Ultra-Dense Carbon Defects as Highly Active Sites for Oxygen Reduction Catalysis. *Chem* **2022**, *8* (10), 2715−2733.
(49) Radovic, L. R. Active Sites in Graphene and the Mechanism of CO_2 Formation in Carbon Oxidation. *J. Am. Chem. Soc.* **2009**, *131* (47), 17166−17175.
(50) Jiao, Y.; Zheng, Y.; Jaroniec, M.; Qiao, S. Z. Origin of the Electrocatalytic Oxygen Reduction Activity of Graphene-Based Catalysts: A Roadmap to Achieve the Best Performance. *J. Am. Chem. Soc.* **2014**, *136* (11), 4394−4403.
(51) Cheon, J. Y.; Kim, J. H.; Kim, J. H.; Goddeti, K. C.; Park, J. Y.; Joo, S. H. Intrinsic Relationship between Enhanced Oxygen Reduction Reaction Activity and Nanoscale Work Function of Doped Carbons. *J. Am. Chem. Soc.* **2014**, *136* (25), 8875−8878.
(52) Sharma, M.; Jang, J. H.; Shin, D. Y.; Kwon, J. A.; Lim, D. H.; Choi, D.; Sung, H.; Jang, J.; Lee, S.-Y.; Lee, K. Y.; et al.etal. Work Function-Tailored Graphene via Transition Metal Encapsulation as a Highly Active and Durable Catalyst for the Oxygen Reduction Reaction. *Energy Environ. Sci.* **2019**, *12* (7), 2200−2211.
(53) Baddorf, A. P.; Rondinone, A. J.; Hensley, D. K. Work Function Measurements of Clean and Modified Carbon Nanospikes. *Carbon* **2020**, *168*, 302−307.
(54) Lee, S.; Hwang, G. S. Valence Force Field-Based Monte Carlo Bond-Rotation Method for the Determination of sp^2-Bonded Carbon Structures. *J. Appl. Phys.* **2011**, *110* (9), 093524.
(55) Perdew, J. P.; Burke, K.; Ernzerhof, M. Generalized Gradient Approximation Made Simple. *Phys. Rev. Lett.* **1996**, *77* (18), 3865.
(56) Kresse, G.; Marsman, M.. Vienna Ab-Initio Simulation Package VASP the GUIDE, VASP Manual: 2014.
(57) Kresse, G.; Joubert, D. From Ultrasoft Pseudopotentials to the Projector Augmented-Wave Method. *Phys. Rev. B* **1999**, *59* (3), 1758.
(58) Blöchl, P. E. Projector Augmented-Wave Method. *Phys. Rev. B* **1994**, *50* (24), 17953.
(59) Dubbeldam, D.; Calero, S.; Ellis, D. E.; Snurr, R. Q. R. RASPA: Molecular Simulation Software for Adsorption and Diffusion in Flexible Nanoporous Materials. *Mol. Simul.* **2016**, *42* (2), 81−101.
(60) Mayo, S. L.; Olafson, B. D.; Goddard, W. A. DREIDING: A Generic Force Field for Molecular Simulations. *J. Phys. Chem.* **1990**, *94* (26), 8897−8909.
(61) Skarmoutsos, I.; Koukaras, E. N.; Klontzas, E. CF_4 Capture and Separation of CF_4−SF_6 and CF_4−N_2 Fluid Mixtures Using Selected Carbon Nanoporous Materials and Metal−Organic Frameworks: A Computational Study. *ACS Omega* **2022**, *7* (8), 6691−6699.
(62) Potoff, J. J.; Siepmann, J. I. Vapor−Liquid Equilibria of Mixtures Containing Alkanes, Carbon Dioxide, and Nitrogen. *AichE J.* **2001**, *47* (7), 1676−1682.
(63) Martin, R. L.; Smit, B.; Haranczyk, M. Addressing Challenges of Identifying Geometrically Diverse Sets of Crystalline Porous Materials. *J. Chem. Inf. Model.* **2012**, *52* (2), 308−318.
(64) Datar, A.; Chung, Y. G.; Lin, L. C. Beyond the BET Analysis: The Surface Area Prediction of Nanoporous Materials Using a Machine Learning Method. *J. Phys. Chem. Lett.* **2020**, *11* (14), 5412−5417.

https://doi.org/10.1021/jacsau.4c00028
JACS Au 2024, 4, 1489−1499